Detection of Psychological Stress Using a Hyperspectral Imaging Technique

Tong Chen, Peter Yuen, Mark Richardson, Guangyuan Liu, and Zhishun She, *Senior Member, IEEE*

Abstract—The detection of stress at early stages is beneficial to both individuals and communities. However, traditional stress detection methods that use physiological signals are contact-based and require sensors to be in contact with test subjects for measurement. In this paper, we present a method to detect psychological stress in a non-contact manner using a human physiological response. In particular, we utilize a hyperspectral imaging (HSI) technique to extract the tissue oxygen saturation (StO2) value as a physiological feature for stress detection. Our experimental results indicate that this new feature may be independent from perspiration and ambient temperature. Trier Social Stress Tests (TSSTs) on 21 volunteers demonstrated a significant difference ($p < 0.005$) and a large practical discrimination (d = 1.37) between normalized baseline and stress StO2 levels. The accuracy for stress recognition from baseline using a binary classifier was 76.19 and 88.1 percent for the automatic and manual selections of the classifier threshold, respectively. These results suggest that the StO2 level could serve as a new modality to recognize stress at standoff distances.

Index Terms—Stress detection, hyperspectral imaging, remote sensing, tissue oxygen saturation

1 Introduction

Human stress represents an imbalanced state [1] of an individual and is triggered when environmental demands exceed the regulatory capacity of the individual [2]. Because of its unhealthy effects [3], stress detection is an ongoing research topic among both psychologists and engineers and has been applied to lie detection tests [4], emergency call identification [5], and the development of better human computer interfaces [6].

Various features associated with stress, including hormone responses, physical appearance, speech, and physiological responses, have been utilized for stress detection. Among these stress features, physiological responses are attracting an increasing amount of attention [7]. However, traditional physiological-based detection methods are contact methods, i.e., sensors must be attached to individuals during feature measurement, which is not convenient for operation.

In this paper, we propose a non-contact detection method that uses a physiological signal. This method enables measurement of a physiological feature at standoff distances, which offers more comfort for test subjects and more covertness for testers.

Specifically, our method uses a hyperspectral imaging (HSI) camera to obtain tissue oxygen saturation (StO2) data as a feature for detecting human stress. In our previous work [8], [9], we discussed a preliminary StO2-generating algorithm that lacked details and exhibited StO2 elevation in only one stressed participant, without statistical results. This pilot study reported, for the first time, that HSI could be a promising technique for remotely sensing human stress. In this paper, we describe the optimized algorithm, elaborate on the experiment design, explain why StO2 was chosen as a stress indicator, present statistical test results, and develop a stress index (SI) to detect psychological stress that is independent of baseline information.

- *T. Chen and G. Liu are with the School of Electronics and Information Engineering, Southwest University, Chongqing 400715, China. E-mail: {c_tong, liugy}@swu.edu.cn.*
- *P. Yuen and M. Richardson are with the Department of Informatics and System Engineering, Cranfield University, Shrivenham, Swindon SN6 8LA, United Kingdom. E-mail: {p.yuen, m.a.richardson}@cranfield.ac.uk.*
- *Z. She is with the School of Engineering, Glyndwr University, Mold Road, Wrexham LL11 2AW, United Kingdom. E-mail: z.she@glyndwr.ac.uk.*

Manuscript received 23 Jan. 2014; revised 18 Aug. 2014; accepted 4 Oct. 2014. Date of publication 9 Oct. 2014; date of current version 2 Dec. 2014. Recommended for acceptance by J. F. Cohn. For information on obtaining reprints of this article, please send e-mail to: reprints@ieee.org, and reference the Digital Object Identifier below. Digital Object Identifier no. 10.1109/TAFFC.2014.2362513

2 Stress Detection: A Review

Various modalities have been employed for the detection of stress, and measuring changes in hormone levels (salivary cortisol) is the approach favored by biologists and psychologists [10], [11], [12]. Kirschbaum et al. [10] observed changes in the cortisol levels of 20 males at the onset of psychological stressors and demonstrated that the cortisol levels of all participants were significantly increased over five day-long experiments. Burke et al. [11] investigated cortisol elevation in response to a stressor under the effects of depressive symptoms and concluded that the stressor triggered a surge in cortisol when individuals were highly depressed. Although the use of cortisol as a biomarker of stress is widely accepted, sample collection requires contact, and the hormone levels must be measured after sample collection. Thus, cortisol-based stress detection is a contact-based and non-real-time detection method.

Inspired by the idea that distinctive human expressions are associated with specific affective states [13], [14], [15], physical appearance (e.g., facial expressions [16], body language [17], eye gaze [18], and blink rate [19]) is commonly utilized as a modality for stress detection. Metaxas et al. [20] presented a model-based system to monitor the deformation of different parts of the face (eyebrows, lips, and mouth) to detect human stress and achieved a true positive

rate of 92 percent or higher. Dinges et al. [16] developed an optical computer recognition algorithm for stress detection by tracking 3D facial expressions (eyebrow movement and mouth asymmetries) that could discriminate high-stress from low-stress performance bouts in 75-88 percent of subjects. Liao et al. [18] employed nine visual features (e.g., blinking frequency, average eye closure speed, percentage of saccadic eye movement) to monitor stress in real-time, and the correlation coefficients between inferred stress and ground-truth stress were between 0.79 and 0.92.

Speech features have also been employed as modalities for stress recognition. Changes in speech characteristics that have been utilized include intensity, duration, pitch, and vocal tract spectrum. In [5], prosodic and spectral features were used to detect the stress level of a caller to distinguish and prioritize urgent calls to an emergency call center. It was reported that the equal error rate of the detection system could reach 4.2 percent.

Physiological features are widely used in stress detection. Human physiological responses to the onset of stressors include increases in heart rate (HR), respiration rate, blood pressure, and body temperature, as well as perspiration, muscle contraction, and pupil dilation. These changes result from the activation of the sympathetic nervous system and cannot be easily suppressed at will [21]. Healey and Picard [22] presented a system called SmartCar to assess a driver's stress level via the analysis of physiological signals, specifically respiration rate, HR, skin conductance, and muscle contraction. The accuracy of the detection was in the range of 62.2-88.6 percent, depending on the combination of features. In [6], blood volume pulse, galvanic skin response, and pupil diameter were used to detect computer users' stress levels, with the goal of providing an improved human-computer interface. The accuracy of stress prediction was from 78.65 to 90.10 percent, depending on the types of classifier used. HR, skin temperature variation, and electrodermal activity were utilized in [23] to assess the affective states related to activation of the sympathetic nervous system. The stress could be differentiated from anger, sadness, and surprise with an accuracy of 61.76-78.43 percent. In general, stress detection based on the measurement of physiological signals using custom or medical meters can provide more accurate results compared with informed guessing. However, this approach for stress detection is impractical in remote sensing applications because sensors must be attached to the test subjects to obtain the physiological signals.

Recently, imaging techniques, such as broadband (webcam) [24] and thermal imaging (TI) [25], have been used for noncontact measurements of physiological signals, including HR [26], [27], respiration rate [24], [28], and HR variability [24]. The noncontact measurement of these physiological signals could be promising for the remote sensing of human stress. However, to the best of our knowledge, no research has evaluated stress detection using this technique. With the exception of HSI, TI is the only method that can remotely probe human stress using physiological features. Distinctive heat patterns in the facial region are assumed to be associated with a specific affective state. Thermal signatures of stress were first observed in 2000 by Pavlidis et al. [29], [30], who reported that an individual's anxiety, alertness, and fear when he/she experienced a sudden startle (physical stressor) were associated with an elevation in temperature around the periorbital region. Following this initial remarkable discovery, Pavlidis [31], [4] confirmed through mock-crime experiments that the detection accuracy of TI was comparable with a traditional polygraph. In TI, skin temperature is presumably modulated by the blood flow in the skin tissue [4], i.e., the increased temperature of the periorbital region is a result of increased blood flow around the area during a stressed state. However, this hypothesis becomes invalid when the ambient temperature changes suddenly. Apart from skin temperature, Shastri et al. [32] proposed that transient perspiration measured by TI could represent a good stress indicator to quantify stress levels. Transient perspiration is a human physiological response and functions well as a stress indicator in most cases. However, we argue that in extreme scenarios where sustained perspiration prevails (e.g., when an individual experiences heavy sweating because of rushing in the airport and must be checked quickly by Future Attribute Screening Technology [33]), transient perspiration cannot be measured. Alternative techniques, such as HSI directly sensing blood oxygenation, can serve as a complementary method for stress detection using physiological responses in a remote sensing manner.

3 HSI

HSI enables the imaging of a scene in hundreds of contiguous, narrow wavebands, with a bandwidth of approximately 10 nm and in the visible and infrared regions of the electro-magnetic spectrum, to form image cubes with both spatial and spectral dimensions [34], [35] as shown in Fig. 1a. Every pixel within the image cube is associated with three coordinates: namely, two spatial coordinates (x,y), which represent the location of pixels in 2D space, and one spectral coordinate (λ), which represents the wavelength. Each pixel in the image cube represents the extent of light reflected by the object in the scene within a narrow slice of wavebands across the whole spectrum, up to the sensitivity limits of the camera. If the intensity of the reflected light is normalized to the incident light intensity for each image pixel, a characteristic reflectance spectrum of the object in the scene can be obtained (Fig. 1b). This technique is very different compared with conventional photography, in which three broad color channels (R,G,B) with wavebands on the order of 100 nm are probed. The integration of spectral characteristics over broad wavebands tends to reduce the color discrimination ability in conventional photography. For this reason, HSI uses a narrow bandwidth for spectral sensing and has been one of the fastest growing technologies in electro-optics in the 20th century. The classification of objects in a scene can be performed using textural features (e.g., shape, orientation, and intensity variation) from a slice of a spectral image (Fig. 1c) or in combination with features selected from a subset of spectral images across different wavebands. Its power of material discrimination [36] is the reason why HSI is used as the primary technique in this research. One requirement of this work is to sense and distinguish blood chromophores from body tissues; the amount of oxygenation within the blood is subsequently quantified using an optical absorption model.

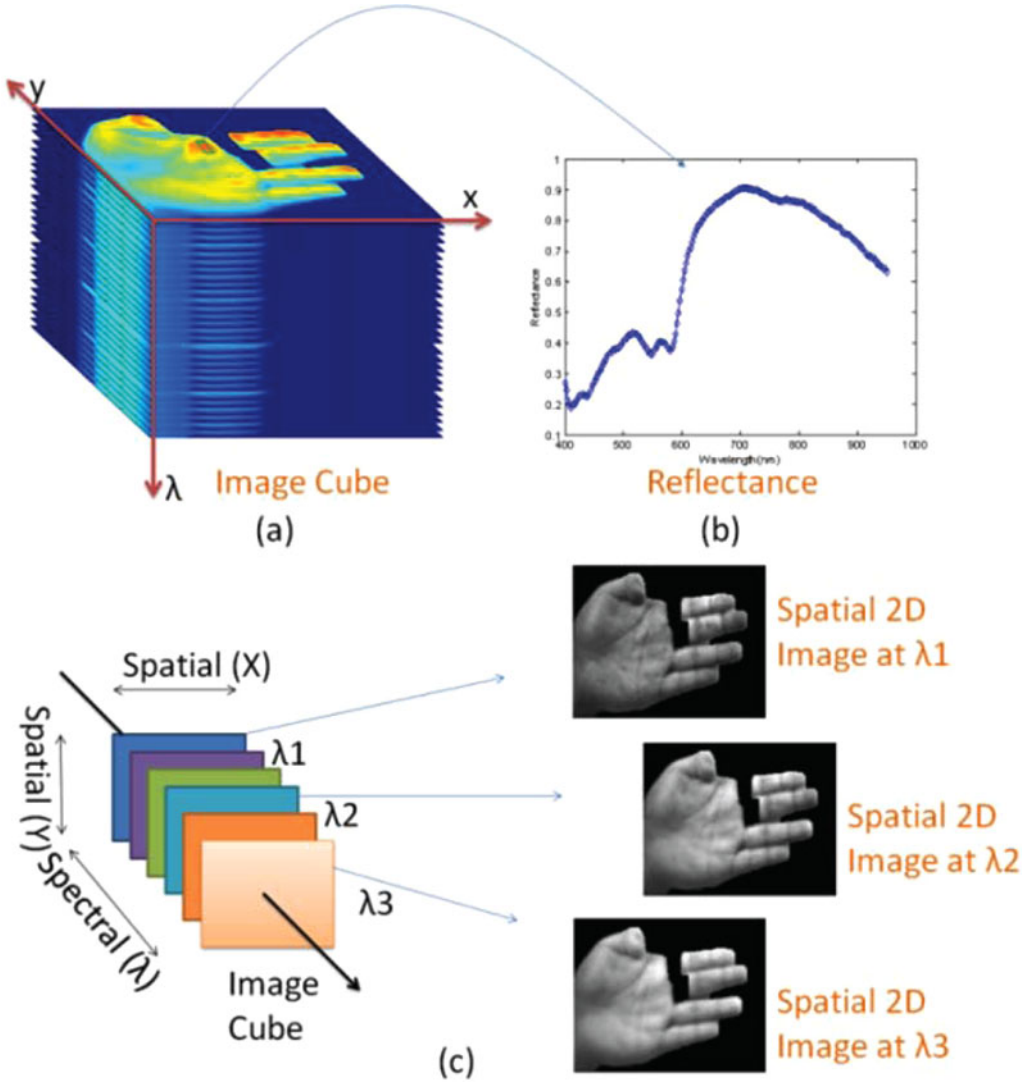

Fig. 1. (a) An HSI image that contains hundreds to thousands of narrow wavebands to form a 3D image cube. (b) The spectral response of the reflectance of palm tissue for all wavebands within a 400-900 nm range. This optical signature is uniquely specific to the chemical composition of palm tissue or the object in question. (c) 2D images of the same object in three different wavebands (palm).

4 Stress and StO2

4.1 StO2

When air is inhaled into the lungs, oxygen binds to hemoglobin through an unstable and reversible bond that forms oxy-hemoglobin (HbO2). HbO2 complexes appear bright red in color and are transported to every part of the body through arterial blood vessels and capillaries. After the oxygen has been consumed by cells and tissues, the HbO2 complexes are decomposed into deoxy-hemoglobin (Hb) complexes, which exhibit a purple-blue color, and are returned to the heart through the venous blood vessels and, subsequently, to the lungs. The next cycle of Hb binding to oxygen to form new HbO2 complexes subsequently begins. Each hemoglobin molecule is capable of binding up to four oxygen molecules. If all four binding sites of each hemoglobin molecule are occupied with oxygen molecules, the oxygen saturation of hemoglobin is 100 percent. However, blood leaving the lung normally has a hemoglobin oxygen saturation range of 90-100 percent, depending on the individual and the situation.

Hemoglobin oxygen saturation (SO2) is defined as the ratio of the amount of HbO2 to the total amount of hemoglobin:

$$SO2 = \frac{HbO2}{Hb + HbO2}. \quad (1)$$

Arterial blood exhibits a relatively strong HR pulsation, and its SO2, which is called the arterial oxygen saturation, is most often measured using the pulse oxymetry technique [37]. Arterial oxygen saturation is fairly constant and varies from 90-99 percent in healthy individuals. StO2 is the SO2 of the microcirculation in tissue and ranges from approximately 60 percent for venous SO2 to 98 percent for arterial SO2 [38], [39].

4.2 Signature of Stress: Arousal of Tissue Oxygenation

Adrenaline is secreted through the hypothalamic-pituitary-adrenal axis in response to a stressor. It binds to the

adrenergic receptors of peripheral tissues, which prepare the body for the fight-or-flight response [40], [41]:

- Acceleration of heart and lung actions.
- Liberation of nutrients, such as glucose and oxygen, for muscular action.
- Increase in blood pressure and stickiness.
- The spleen discharges red and white blood cells, which enables the blood to transport more oxygen throughout the body. Blood flow can increase by up to 300-400 percent, which primes the muscles, lungs, and brain for added demands.
- Redirection of blood to provide the highest perfusion and fuel to the aroused brain, heart and muscles.

These responses substantially increase the StO2 and tissue oxygen content. An experiment that involves the controlled infusion of adrenaline into human forearms [42] with variable doses demonstrated that the SO2 of venous blood draining from the forearm muscle experiences a significant transient increase that is independent of the dose, which indicates a transient increase in the muscle StO2 or tissue oxygen content [43]. The response after the transient increase is dose-dependent. A smaller dose ($0.05\mu g/min$, $0.1\mu g/min$ intra-arterial infusion) induces a sustained increase in the venous SO2, whereas a larger dose ($0.2\mu g/min$, $0.5\mu g/min$ intra-arterial infusion) tends to decrease the oxygen saturation of the superficial skin of the forearm (in capillary vessels).

A high amount of adrenaline infusion, $2\mu g/kg$ per minute, was employed in [44] to investigate the oxygen usage of the heart muscle in dogs. The oxygen extraction of the muscle decreases, whereas the oxygen consumption slightly increases, during the infusion. These effects result in an increase in the muscle StO2 throughout the period of infusion.

A transient increase in blood flow, which indicates a transient increase in oxygen saturation, in the rat masseter muscle after intravenous infusion was observed in a recent experiment [45]. The response of blood flow after the initial rise was also dose-dependent (i.e., a larger dose decreased the blood flow more). This experiment also suggests that adrenaline secreted from the adrenal gland has a similar effect on the masseter oxygen saturation.

The effects of increased superficial blood flow (1-2 mm [46] below the skin surface) on the human facial region upon the onset of a psychological stressor was recently reported. The mean blood flow (measured by laser Doppler flowmetry or photoplethysmography) of the forehead [46], [47], [48] and cheek [47], [48] during the stressed state increases, which reveals that the StO2 of these regions is affected by the stress or the hormones secreted along with the stress.

From these previous publications, it is clear that the stress hormone adrenaline or stress itself can trigger higher oxygen saturation (content) in certain tissues (including facial tissues), although the increase can be transient or sustained. In the case of very short-term increases, the post-transient response may be influenced by the amount of adrenaline and the severity of the stressor. Very large amounts of adrenaline or sustained stimulation of the adrenal medulla may lead to the maintenance of higher tissue oxygenation levels.

5 Methodology for StO2 Assessment Using HSI

HSI is an emerging technique used to remotely sense StO2 in vitro, and the results can be presented in a spatial 2D StO2 map. Substantial efforts [49], [50], [51] in the field of HSI StO2 assessment have been based on the Beer-Lambert Law, which relates the absorption of light to the properties of the material through which the light is traveling:

$$A = \varepsilon lc, \tag{2}$$

where A is the absorbance, ε defines the molar extinction coefficient $cm^{-1}(\frac{mol}{L})^{-1}$ (or molar absorptivity) of the material, c represents the molar concentration (mol/L) of the absorber, and l denotes the distance (cm) traveled by the light through the material. In an HSI reflectance model, the path length l is difficult to measure. The product lc in equation (2) is thus reduced to C_{eff}, the effective concentration ($10^{-3}mol/cm^2$), which represents the molar concentration of absorbers per unit area.

The absorbance in this work is deduced from the diffuse reflections of body tissue using the equation

$$A_\lambda = \ln \frac{1}{R_{\lambda\_Total} - R_{\lambda\_Specular}}, \tag{3}$$

where A_λ, R_{λ_Total}, and $R_{\lambda\_Specular}$ are the absorbance, total reflectance, and specular reflectance values of skin tissue, respectively. The wavelength-dependent R_{λ_Total} is obtained through the empirical line method (ELM) as follows:

$$R(x, y, \lambda) = a_\lambda I(x, y, \lambda) + b_\lambda, \tag{4}$$

where $I(x, y, \lambda)$ is the intensity of pixel (x, y) at wavelength λ, and a_λ (from 0.003 to 0.04) and b_λ (from -1 to -0.02) are calibration coefficients extracted from standard reflection material (spectralon)

$$R_{White\_\lambda} = a_\lambda I_{White\_\lambda} + b_\lambda, \tag{5}$$

$$R_{Black\_\lambda} = a_\lambda I_{Black\_\lambda} + b_\lambda, \tag{6}$$

where I_{White_λ} and I_{Black_λ} are the mean pixel intensities of the white and black spectralons, respectively, at wavelength λ, and R_{White_λ} and I_{Black_λ} denote the reflectance values of the white and black spectralons, which are 0.98 and 0.02, respectively, over spectral region of 250-2500 nm.

The specular reflectance $R_{\lambda\_Specular}$ is the ratio of specular reflected light intensity from the skin surface to the total incident light intensity. This value is determined by subtracting the tissue body reflectance [52] from the total reflectance. The tissue body reflectance is calculated using the same method used to obtain the total reflectance, with the exception that two cross-polarized polarizers are required to be placed in front of the illumination source and the HSI sensor during measurement recording [49]. The specular reflectance of skin tissue used in this research is shown in Fig. 2.

The chromophores considered in this research are Hb, HbO2, and melanin. Thus equation (2) becomes

$$\begin{aligned} A = {} & \varepsilon_{HbO2}\mathcal{C}_{effHbO2} + \varepsilon_{Hb}\mathcal{C}_{effHb} \\ & + \varepsilon_{melanin}\mathcal{C}_{effmelanin} + G, \end{aligned} \tag{7}$$

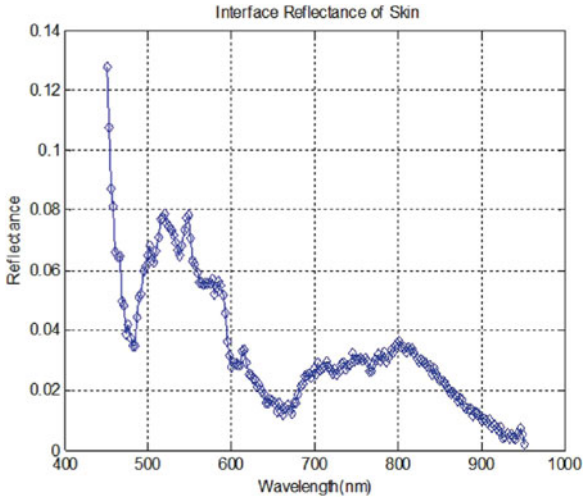

Fig. 2. Interface (specular) reflectance of skin over the wavelength range of 450-950 nm.

where ε_{HbO2}, ε_{Hb}, and $\varepsilon_{melanin}$, and $\mathcal{C}_{effHbO2}$, $\mathcal{C}_{effHb}$, and $\mathcal{C}_{effmelanin}$ are the molar absorptivities and the effective concentrations of HbO2, Hb, and melanin, respectively. The term G represents a collection of photons that have been scattered out of the sensor's view angle. In this research, the values of ε_{HbO2}, ε_{Hb}, and $\varepsilon_{melanin}$ were adopted from literature [53], [54].

The estimated effective concentrations of $\mathcal{C}_{effHbO2}$ and $\mathcal{C}_{effHb}$ from equation (7) are strong indicators of real molar concentrations of HbO2 and Hb. the deduced $\mathcal{C}_{effHbO2}$ and $\mathcal{C}_{effHb}$ values were previously identified, by solving equation (7), to be linearly proportional to the real concentrations of HbO2 and Hb, with correlation coefficients of 0.86 and 0.88, respectively [49]. This correlation makes $\mathcal{C}_{effHbO2}$ and $\mathcal{C}_{effHb}$ increasingly useful in diagnostic and clinic applications, such as predicting the risk of diabetic foot ulcer formation [49], visualizing kidney StO2 during open partial nephrectomies [55], and distinguishing superficial burn wounds from deep wounds [56].

In theory, sets of values of A, ε_{HbO2}, ε_{Hb}, and $\varepsilon_{melanin}$ at three or more wavelengths can determine the $\mathcal{C}_{effHbO2}$ and $\mathcal{C}_{effHb}$. Thus, various groups of wavelengths equally distributed over the visible and near infrared range have been employed for StO2 assessment by different researchers [49], [50], [51]. In this paper, wavelengths from 518 to 580 nm with a step size of 2 nm were selected to deduce StO2 because we have demonstrated that this spectral region can provide more robust StO2 results in terms of illumination independence and accuracy [57].

Because each StO2 map pixel is affected by the surrounding tissue, the final StO2 map is generated after the raw StO2 map is averaged.

6 Comparison of HSI and TI for the Assessment of StO2

6.1 Research Motivation

Both HSI and TI techniques can assess StO2, either directly or by measuring skin blood perfusion [58], which enables the monitoring of StO2 at standoff distances without requiring contact with the target tissue. In this section, we examine how these two technologies perform in the assessment of StO2 under normal conditions, where the ambient temperature is constant and the body temperature scheme is not dominant, as well as in extreme conditions, where the ambient temperature experiences a $15^{\circ}\mathrm{C}$ change or perspiration prevails. The ambient temperature (see Section 6.4) and perspiration (see Section 6.5) effect tests were performed on four test subjects (three males, one female; $\mathrm{N} = 2$ or 3), and the results were consistent.

6.2 Instrumentation and Experimental Setup

The HSI system utilized in this research consisted of a Headwall VNIR spectrograph (HeadWall VNIR, USA) combined with a PCO PixelFly camera (PCO PixelFly, Germany) and a home-designed mirror scanning system. The slit of the spectrograph was 30 μm wide, which provided a maximum spectral resolution of $\sim$5 nm. The spectral sensitivity limit of the PCO camera ranged from 400 to 1,000 nm, with a maximum quantum efficiency yield of $\sim$65 percent at $\sim$650 nm. The opening angle of the PCO camera was 30 degree. The dimensions of the entire HSI system were approximately $40 \times 40 \times 15$ cm. The TI system consisted of a FLIR SC7600 mid-wave infrared camera for skin temperature measurements, with a temperature resolution of $0.02^{\circ}\mathrm{C}$ and a working range of -20 to $+100$ $^{\circ}\mathrm{C}$. Broad-band halogen lamps were used throughout the imaging process as illumination sources. The two imaging systems, i.e., HSI and TI, were placed 2-3 m away from the objects. A chest-strap heart monitor (Garmin, USA) was used to monitor the HR of each subject during the experiment.

The HSI system took pictures using a fixed number of wavelengths, which ranged from 400 to 1,000 nm in 2 nm steps (300 wavelengths). This system required 10 s (integration time 40 ms, 250 scanning lines) to record one image cube. The StO2 measurements result from the still images of the objects.

The HSI system used in this research cannot operate in real-time. However, by using a more-sensitive HSI system (integration time can be 5 ms) with the ability to image a flexible number of wavelengths, such as an acoustic-optic tunable filter-based [59] HSI system with scientific CMOS or electron multiplying CCD sensors, the image cube could be obtained in approximately real-time (8 fps, if 30 wavelengths within 520-580 nm were used).

6.3 Consistency of HSI StO2 and TI Temperature

Skin temperature is modulated by StO2, and it was assumed that the ambient temperature and metabolic rate were stable and that no body temperature regulation methods, such as perspiration, were dominant. To verify that the change in HSI StO2 was consistent with the change in TI temperature, and vice versa, an ischemia experiment was performed. Ischemia assessments that use HSI have been reported to demonstrate the effectiveness of the technique for detecting HbO2 [60], [61]. In this work, we compared the StO2 assessment from the HSI data with the skin temperature, measured with TI, of ischemic tissues. An ischemic state was introduced to the forefinger and middle finger of the palm of a healthy volunteer by wrapping the two fingers with a tight rubber band for three minutes. After the ischemic

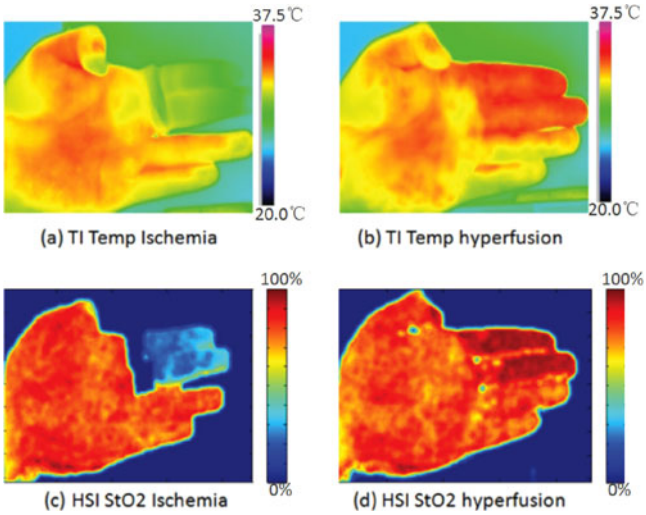

Fig. 3. TI temperature and HSI StO2 maps of a palm with two fingers in ischemic and hyperperfusion states. (a) A TI temperature map that measures a palm with two fingers in an ischemic state; (b) a TI temperature map that measures a palm with two fingers in a hyperperfusion sate; (c) an HSI StO2 map that measures a palm with two fingers in an ischemic state; and (d) an HSI StO2 map that measures a palm with two fingers in a hyperperfusion state.

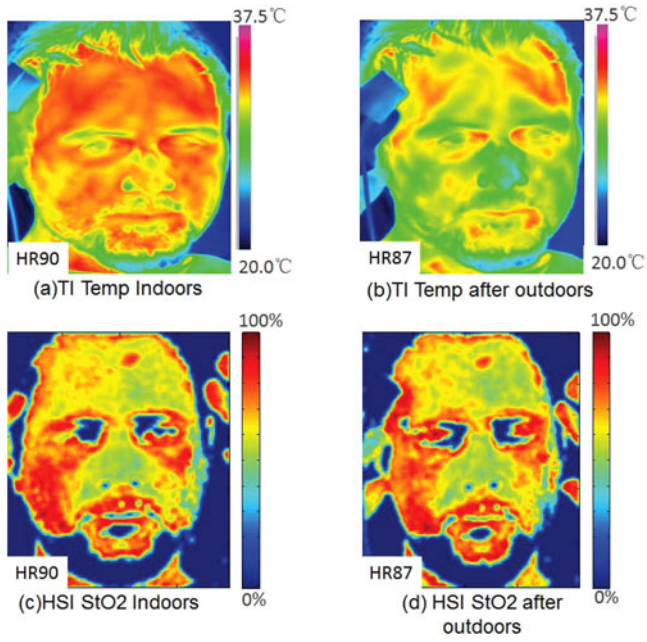

Fig. 4. TI temperature and HSI StO2 maps of the same human face in warm and cool environments. (a) A facial temperature map in an indoor environment. The heart rate of the subject was 90 bpm at the moment that the TI data were recorded; (b) a facial temperature map obtained immediately after returning from an outdoor environment (HR was 87 bpm); (c) a facial StO2 map in an indoor environment (HR was 90 bpm); and (d) a facial StO2 map obtained immediately after returning from an outdoor environment (HR was 87 bpm).

finger images had been captured via TI and HSI, the rubber band was removed, which caused fresh blood to flush into the two fingers and induce immediate hyperperfusion.

As shown in Fig. 3, the changes in the StO2 and temperature of the two fingers were consistent with each other. The skin temperature and StO2 of the ischemic fingers decreased by approximately $4°C$ and 55 percent, respectively, compared with the undisturbed fingers of the other palm. The fingers that experienced hyperperfusion exhibited increases of $1°C$ and 20 percent in skin temperature and StO2, respectively, compared with the normal palm. Notably, as shown in Fig. 3, the skin temperature correlated very well with the StO2 over the entire palm.

6.4 Ambient Temperature Effect

Two different ambient temperatures were introduced in a controlled experiment to examine how StO2 and skin temperature are modulated by the temperature of the environment. In this experiment, the subjects were requested to comfortably and calmly sit on a chair in a laboratory environment with a room temperature of $20°C$ for 1 hour. TI and HSI data were recorded when their HR reached a stable state during this time period (a TI frame was obtained during the HSI exposure). The subjects were then asked to walk outside for 10 minutes, where the temperature was approximately $5°C$. TI and HSI data were recorded again, as soon as the subjects returned from the outside environment.

Fig. 4 illustrates the facial temperature and StO2 maps of a subject. The top panel of the figure represents temperature, and the bottom corresponds to StO2. The left column displays the maps obtained in an indoor environment, and the right column shows the maps obtained immediately after returning from an outdoor environment. The HR of the subject at the time when the TI and HSI data were recorded is shown at the bottom left corner of each map.

The HR of the subject was stable throughout the experiment, which indicates the body blood circulation was nearly constant. However, the large temperature difference between the indoor and outdoor environments caused an abrupt decrease in the facial skin temperature and, more notably, in the nose region, with a reduction of $8°C$ observed after the subject returned from outside (Fig. 4b). The skin temperature in the face recovered after 10 minutes of rest in an indoor environment ($20°C$) after the event. In contrast to the skin temperature measurements, the StO2 levels remained fairly stable after the subject returned from outside (Fig. 4d). The StO2 in the forehead region decreased by a negligible 0.2 percent of the indoor value, presumably due to the constriction of blood vessels after being in a cold outdoor environment for 10 minutes.

Twenty-five small facial regions were selected for analyses, as shown in Fig. 5. The average HSI StO2 and TI temperature values of the regions were calculated. An analysis using Student's t-test revealed a significant difference ($p < 0.005$) between the TI facial temperatures for the indoor (mean = 33.67, stdev = 0.37) and outdoor (mean = 32.00, stdev = 1.26) measurements, and Cohen's d indicated a large practical difference (d = 1.24). However, no significant difference was identified between the HSI StO2 levels ($p > 0.05$) for the indoor (mean = 65.22, stdev = 8.71) and outdoor (mean = 64.79, stdev = 7.88) situations.

6.5 Perspiration Effect

To induce a state of perspiration, the subjects were asked to conduct exercises in a warm indoor environment until they began to sweat. The baseline (calm state before exercise)

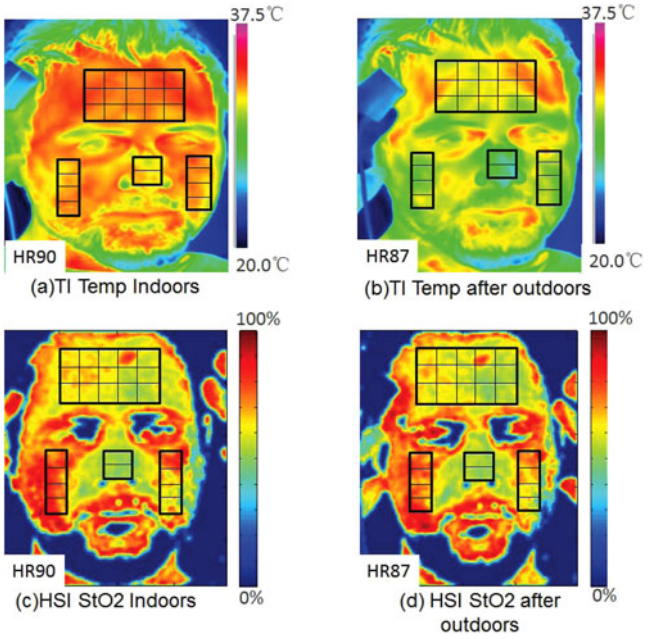

Fig. 5. Twenty-five small regions selected on a subject's face for comparison.

and sweat conditions of TI and HSI data were recorded. In general, blood perfusion in the facial region increases after moderate physical exercise [8], [62], [9].

Fig. 6 shows the StO2 and temperature maps in the bottom and top panels, respectively. The maps for a test subject that demonstrated the baseline state, the perspiration condition after exercise, and the condition 8 minutes after perspiration are shown in the left, middle, and right columns, respectively. The HR of the subject is shown in the bottom left corner of each map.

Perspiration reduced the skin temperature by $5°C$, which corresponded to an $\sim$11 percent decrease with respect to the baseline state in particularly sweaty regions (Fig. 6). In contrast to the skin temperature measurements, the StO2 in the forehead increased by $\sim$3.2 percent from baseline, which typically occurs because of increased physical activity, increased HR, and perhaps adrenaline in the blood stream [8], [62], [9].

The heavy sweat observed in the forehead regions (Fig. 6) does not appear to decrease the StO2 measured from the HSI data, which is in contrast to the effect observed on the skin temperature measurements. The central forehead region of the subject in Fig. 6 (i.e., from the end of the left eyebrow to the end of the right eyebrow and from the top of the eyebrows to 2/3 the distance from the top to the bottom of the head), which contained 3000 ± 500 pixels, was selected to produce the average and standard deviation values of StO2 and temperature. These values are shown in Fig. 7. The data demonstrated the average forehead StO2 continuously increased. However, because of sweat, the forehead temperature after exercise was substantially lower compared with the baseline temperature and did not recover to the baseline value, even 8 minutes after the cessation of exercise.

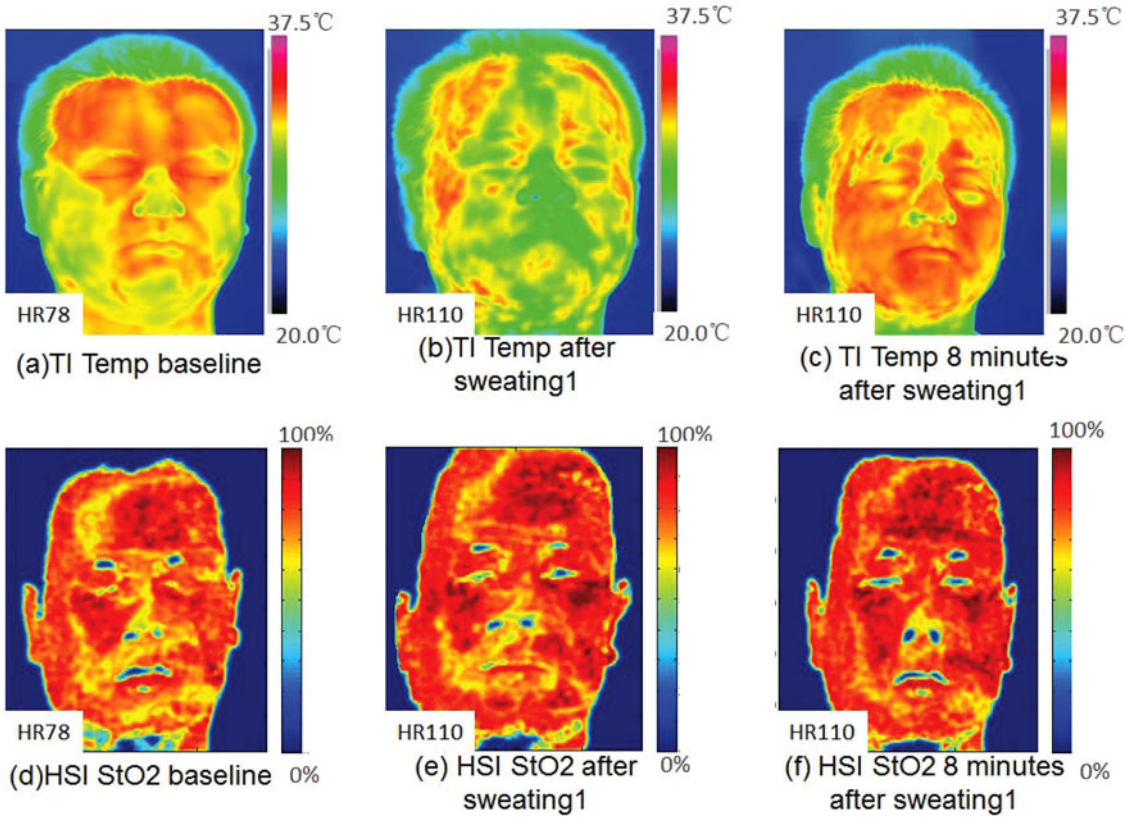

Fig. 6. TI temperature and HSI StO2 maps of the face of a healthy subject under baseline and sweating conditions.(a) A baseline facial temperature map (HR was 78 bpm); (b) a sweat condition facial temperature map (HR was 110 bpm); (c) a facial temperature map obtained 8 minutes after obtaining (b) (HR was 110 bpm); (d) a baseline facial StO2 map (HR was 78 bpm); (e) a sweat condition facial StO2 map (HR was 110 bpm); and (f) a face StO2 map obtained 8 minutes after obtaining (e) (HR was 110 bpm).

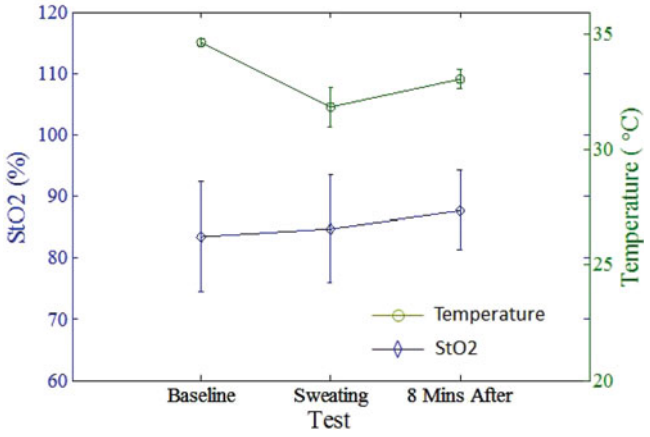

Fig. 7. Average StO2 and temperature of the central forehead region in Fig. 6.

7 Detection of Stress With HSI StO2

7.1 Psychological Stressors

A slightly modified Trier Social Stress Test (TSST) [63] was used in this study to trigger acute psychological stress. The stressors (e.g., public speaking and mental arithmetic) in a standard TSST share characteristics of exposing participants to a social-evaluative threat and a state of expecting an uncontrollable performance outcome. These characteristics are the most important elements for triggering strong stress responses with respect to cortisol release [64]. In addition to public speaking and mental arithmetic, we used an additional stressor in this study. Considering that some participants may be good at presentations and mental arithmetic, their stress responses may not be triggered. Thus, recognition-memory tasks were used as a complementary stressor, and the uncontrollable and social-evaluative characteristics of these tasks were carefully designed.

In the mental arithmetic test, each participant was asked to perform mental calculations for 25-30 simple arithmetic problems and was required to provide the answers within a tight time scale of 4-5 seconds. The participants were first informed of the expected score prior to administering the test to impose a psychological pressure. The test was designed in such a way that a gradual increase in question difficulty was initiated during the middle of the session, thereby gradually increasing the psychological pressure.

In the public speaking test, each participant was asked to deliver a presentation in front of a panel of referees and interviewers. The presentation could be in the form of a job interview or a project description. Prior to the test, the participant was told that the presentation would be videoed and subsequently analyzed to evaluate the presentation style and nonverbal signals. A detailed description of the stressors of public speaking and mental arithmetic has previously been provided [63].

In the memory test, each participant was asked to remember a set of two images that appeared together in the same PowerPoint slide. In the learning session, a series of image pairs flashed up and then remained on the screen for 2 seconds. After flashing approximately 6-10 slides of images, the participants were asked to identify which two of the five images that appeared on a given test slide were in a previously shown pair. The participants were required to respond to each test slide within a time limit of 5 seconds. Furthermore, they were told prior to the test that their hit rate (number of correct answers) would be recorded for comparison with the average hit rate derived from the responses of all the participants.

7.2 Saliva Cortisol and HR as Indicators of Stress Response

Cortisol is a reliable biomarker for acute psychological stress [65]. Therefore, saliva cortisol served as an accurate basis to judge whether the stress response was activated in this study. The participants' cortisol levels at baseline and after each stress testing cycle were compared. Only when a participant's stress cortisol level increased to at least 125 percent of his/her baseline cortisol level could he/she be regarded as a successfully stressed participant, and his/her HSI data at the end of the stress test were used for subsequent analyses.

A small cotton swab of a salivette [65] was provided to each participant prior to conducting the stress test (baseline) and retrieved after the test. The participants were advised to chew the swab gently during the test so that the swab could sample sufficient saliva, which was subsequently sent to a hospital for cortisol level assessment.

We did not continuously record HSI data; therefore, we had to be informed of when a participant began to feel stressed to initiate the HSI data recording. However, during the stress test, we could not judge whether the participants were experiencing the stress response by analyzing their cortisol level; this analysis was performed after testing. Fortunately, the TSST elevates not only cortisol levels but also HR [66]. Therefore, HR elevation served as an indicator for recording and monitoring HSI data throughout testing. A rise in HR was presumed to indicate that a participant was stressed, and his/her HSI data recording was initiated when a continuous rise in HR was observed from the previous time point and when his/her HR was at least 6 beats per minute (bpm) higher compared with the HR at the beginning of the test (Fig. 8).

7.3 Experimental Procedures and Protocols

The three psychological stressors for inducing stress in this work were mental mathematics, public speaking, and recognition-memory tasks. One or all of these mental stimulations were applied to each participant until an increase in HR (continuous rise and at least a 6 bpm increase compared with the initial HR) was observed. The stressors applied to the participants were sequential: the mental arithmetic test, the memory test, and then public speaking.

Twenty-one healthy volunteers (subjects A-U, mean age of 25) exhibited a positive stress response according to the saliva cortisol analyses. The participants were students and staff of Cranfield University, from various origins and career backgrounds, and were recruited for the stress sensing experiment. Nineteen volunteers were male and two volunteers were female. The large percentage of male participants in this study was a result of the constraints of sampling from a predominantly male institute, which is typical of a national defense college.However, the effect of gender on the StO2 response to a psychological stressor is not currently known. The experimental procedure for this research

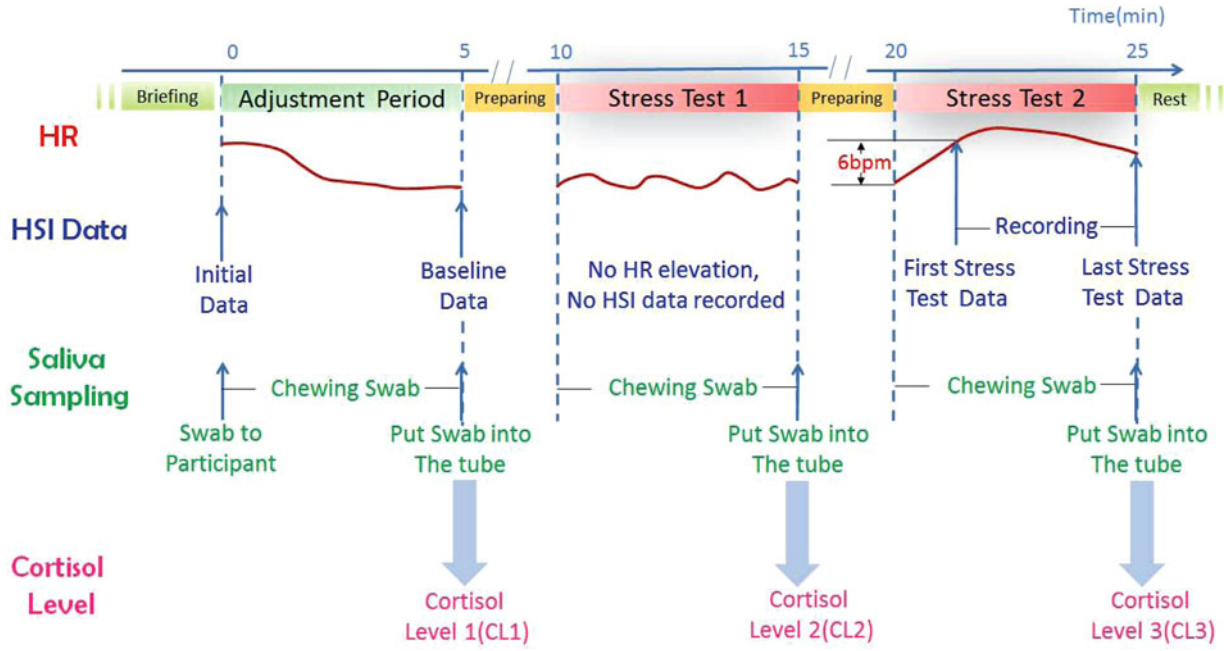

Fig. 8. Experimental procedure.

was approved by the UK National Health Service Research Ethics Committee (REC reference: 09/H0107/2), and consent from the participants was obtained prior to the experiment. Halogen lamps were used as the sole illumination source of the scene, with an intensity of approximately 500 lux at the target. The room was air conditioned according to the REC procedure. A typical testing sequence is illustrated in Fig. 8 and described as follows:

The participants were invited to participate in the experiment, and an explanation of the general experimental procedures was provided.

At 0 min, the facial HSI data of the participant were recorded, and the participant was then required to sit calmly and comfortably for 5-10 minutes. The participant's affective state varied at the beginning of the experiment (0 min: the time at which the participant entered the laboratory). Thus, we named this affective state the Initial Affective State, and the HSI data recorded at the time of 0 min were termed initial data. At the end of the adjustment period and when the participant's HR reached a stable reading, the facial HSI data were again recorded, which served as the baseline (calm) information. A cotton swab was chewed by each participant throughout the adjustment period and was retrieved at the end of testing for cortisol level analysis.

Each participant was given another 5 minutes to prepare for stressor 1, i.e., they were informed of the specific procedure and the requirements of stressor 1.

Stressor 1, one of the psychological stressors described in Section 7.1, was then administered to the participant. If no obvious HR elevation was observed, the HSI data were not recorded during testing. The saliva sample was obtained in a manner similar to the adjustment period.

Another five minutes was given to the participant to prepare for stressor 2.

Stressor 2 was then administered to the participant. If he/she experienced a continuous rise in HR, the HSI data were recorded, starting when the HR was at least 6 bpm higher compared with the HR at the beginning of testing. The HSI data were continuously recorded at 30-60s intervals. At the end of stressor 2, the HSI data were recorded for the last time. A saliva sample was again obtained. The last set of HSI data served as the potential stress data, considering that the saliva sample was obtained immediately after HSI recording.

The participant was told that his/her presentation style and nonverbal signs would not be analyzed, that their expected score/hit rate was much higher than average, and that he/she performed well in the arithmetic and memory tests. A rest period of approximately 10-20 minutes was then allowed.

As previously shown [67], [63], cortisol levels rise to ~125 percent of baseline cortisol levels after 5 minutes of stress testing. Therefore, in this study, if the cortisol level (CL3 in Fig. 3) measured at the end of the stressor 2 test was at least 1.25 times as high as the baseline cortisol level(CL1 in Fig. 3), the HSI data recorded at the end of the stressor 2 test were regarded as the stress information data for the participant.

If the HR elevation during the stressor 1 test triggered HSI data recording, the stressor 2 test was not administered to the participant. If the HR elevation was not observed during either stress test, a stressor 3 test was administered.

During the stress test, the participant was not required to remain still. However, the participant was asked to sit still when his/her initial data, baseline, and last stress test data were recorded (Fig. 8). These HSI data were subsequently used for stress detection.

7.4 Facial StO2 and Stress Detection

The StO2 results indicated that all 21 participants exhibited an increase in StO2 level in the facial region, particularly in the forehead region, when subjected to a psychological stressor. Figs. 9a and 9b show the facial StO2 maps of participant A at baseline and when a psychological stressor was experienced, respectively. The average HR of the

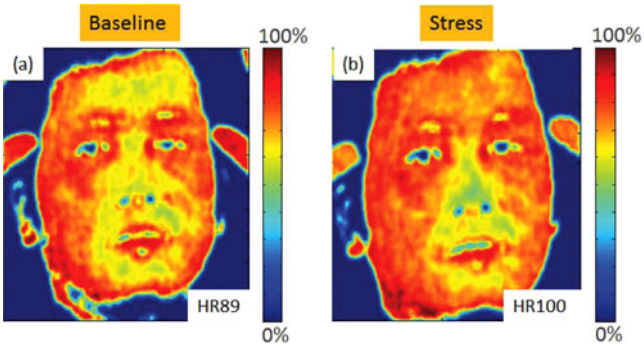

Fig. 9. StO2 maps of participant A (a) at baseline and (b) when psychological stress was experienced.

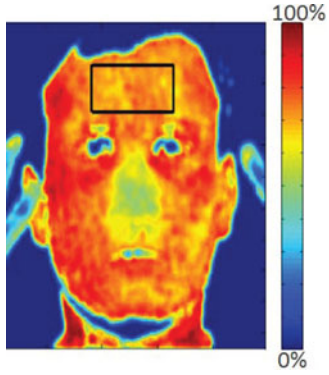

Fig. 10. Region of interest on the forehead for generating the average and standard deviation StO2 values.

participant at the moment of HSI recording is shown in the bottom right corner of each image.

Participant A exhibited an increase in tissue oxygenation in the facial region, particularly in the forehead and eye socket regions, when a psychological stressor was experienced. This facial StO2 elevation was observed in all 21 participants when stress was experienced.

To investigate how the StO2 levels change due to psychological stressors, the average StO2 levels of 11 regions of interest (ROIs) in the face were studied. However, only the StO2 forehead values of the 21 participants are highlighted here because the other results are not allowed to be released at this time. The forehead ROI used to calculate the average StO2 levels was the forehead center region (i.e., from the end of the left eyebrow to the end of the right eyebrow and from the top of the eyebrows to 2/3 the distance from the top to the bottom of the head), which is highlighted in Fig. 10 with a black rectangle. Because of individual differences, the ROI contains 3000 ± 500 pixels. Each pixel has an StO2 value, and one ROI can therefore produce an average StO2 and a standard deviation value.

The average ROI StO2 values as well as the standard deviations, rates of StO2 increases, HR increases, cortisol increases as a result of the stressors, and stressors used for triggering the stress response (i.e., a rise in cortisol) for each participant are summarized in Table 1. Due to the different physiques of each individual, the average baseline forehead StO2 values of the participants span from as low as 50 percent (participant M) to as high as 84 percent (participant O). All HRs and cortisol levels of the participants increased, which ranged from a minimum elevation rate of 3.41 percent for HR (participant H) and 16.49 percent for cortisol (participant B) to a maximum of 33.33 percent for HR (participant T and L) and 196.13 percent for cortisol (participant A); these findings indicate positive responses to the stimulations from all participants. As shown in Table 1, all participants experienced StO2 elevation during psychological stress, from a minimum elevation rate of 1.5 percent (participant L) to a maximum of 28 percent (participant I).

A boxplot of the average ROI StO2 under baseline and stress states is shown in Fig. 11. The difference in StO2

TABLE 1
Average(Avg) StO2 Values and Standard Deviations (Std) from Forehead ROIs for 21 Participants

Participant	Baseline(B)		Stress(S)		StO2	HR	Cortisol	Stressor
	Avg StO2 (%)	Std StO2 (%)	Avg StO2 (%)	Std StO2 (%)	Increase Rate (%)	Increase Rate (%)	Increase Rate (%)	Used
A	64.14	5.43	72.01	3.24	12.27	12.36	196.13	Math
B	65.77	4.18	77.04	2.94	17.14	12.35	16.49	Math
C	61.64	5.45	67.63	3.02	9.72	19.57	39.31	Speech
D	72.52	6.00	80.23	5.26	10.63	30.43	62.83	Memory
E	73.24	4.14	78.60	5.60	7.32	10.13	45.37	Math
F	70.81	4.04	73.33	3.51	3.56	20.00	25.62	Memory
G	66.69	3.63	70.03	3.88	5.01	7.04	52.38	Math
H	68.79	3.26	75.46	2.69	9.70	3.41	91.77	Memory
I	56.07	5.66	71.97	4.01	28.36	9.23	42.29	Memory
J	60.16	6.36	72.96	4.58	21.28	5.62	61.34	Memory
K	77.01	3.83	80.96	3.83	5.13	13.33	30.24	Memory
L	78.05	4.09	79.22	3.28	1.50	33.33	155.78	Memory
M	50.10	5.07	59.11	5.23	17.98	6.67	271.10	Math
N	75.05	6.96	76.54	6.41	1.99	8.96	68.47	Memory
O	84.12	4.80	90.70	3.12	7.82	4.17	114.66	Math
P	78.29	4.71	80.83	4.55	3.24	12.50	32.64	Math
Q	67.25	4.76	71.70	4.09	6.62	15.38	28.41	Memory
R	68.48	3.26	76.72	4.09	12.03	19.05	44.96	Memory
S	63.29	3.26	71.20	4.37	12.50	7.14	27.44	Memory
T	75.96	6.37	82.85	4.86	9.07	33.33	57.19	Math
U	68.92	4.93	74.98	4.01	8.79	26.23	43.70	Math

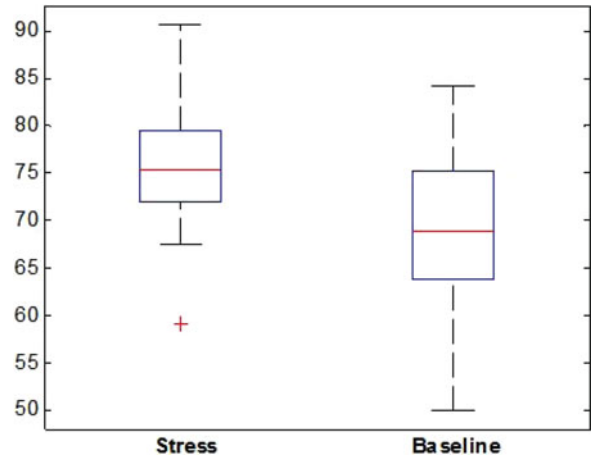

Fig. 11. Box plots of the average ROI StO2 under baseline and stress states.

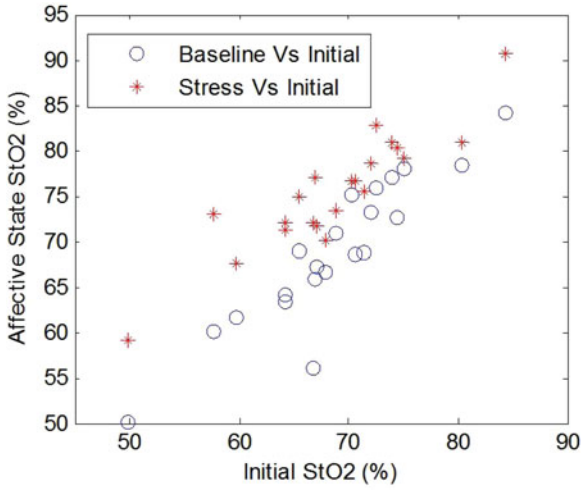

Fig. 12. Scatter plot of Stress StO2 vs. Initial StO2 and Baseline StO2 vs. Initial StO2 for 21 participants.

between these two states is intuitive from the boxplot. A one-tailed paired Student's t-test identified a significant difference ($p < 0.005$) between the average forehead StO2 values for the baseline (mean = 68.87, stdev = 8.10) and stress (mean = 78.43, stdev = 6.41) conditions, and Cohen's d indicated a large practical difference (d = 0.83). This significance suggests that forehead StO2 values are good stress indicators.

However, using forehead StO2 directly as a parameter to discriminate stress from baseline states is not practical. The stress and baseline StO2 values of the different participants are not directly comparable because of the physiological differences between the individuals. As shown in Table 1, although the stress StO2 of each participant was always higher compared with his/her baseline StO2, it was lower compared with the baseline StO2of other participants in some cases. For example, the stress StO2 of participant C was lower compared with the baseline StO2 of participant D, and the stress StO2 of participant M was lower compared with the baseline StO2 of most other participants.

To eliminate the effects of individual differences and make StO2 a useful stress indicator, the StO2 values must be normalized from a statistical point of view (i.e., the raw StO2 values from different individuals must be normalized to standard values so that the StO2 values from different individuals are comparable). In this study, we employed the average forehead initial state StO2 values as a reference for transformation. Fig. 12 shows a scatter plot of the affective state StO2/initial StO2 values. The affective states here include stressed and baseline states, which can be discriminated from each other. In Fig. 12, the stress and baseline values are grouped into two distinct clusters.

Based on the previously described observations, we calculated the ratios of the StO2 for each participant with respect to his/her initial StO2 to obtain a SI. For the 21 participants, 42 SIs were generated, which included 21 SIs for the stress state (mean = 1.10, stdev = 0.06) and 21 SIs for the baseline state (mean = 1.00, stdev = 0.05). A one-tailed paired Student's t-test identified a significant difference ($p < 0.005$) between the stress and baseline SIs, and Cohen's d indicated a large practical difference (d = 1.37).

We then employed a binary classifier to identify the stress state. By selecting different thresholds, a classifier receiver operating characteristic (ROC) curve for the classifier can be generated, as illustrated in Fig. 13. The most conservative classification with the best performance was identified at the point (0, 0.619) in Fig. 13. The classification accuracy at (0, 0.619) was 80.95 percent, and the highest classification accuracy of 88.1 percent was observed at the point (0.1905, 0.9524),where the true positive and false positive rates were 95.24 and 19.05 percent, respectively. The threshold automatically obtained from Otsu's algorithm [68] was 0.9216. In this case, the true positive rate, false positive rate (circle in Fig. 13), and accuracy were 95.42, 42.86, and 76.19 percent, respectively.

Because of the limited number of participants, the classification results presented are participant-dependent and vary between the participant groups. However, the classification threshold should approach a stable constant if large groups of data are used.

To investigate how the StO2 reactivity correlates with the HR and cortisol reactivity, we created scatter plots of the StO2 increase rate versus the HR increase rate (Fig. 14a) and the StO2 increase rate versus the cortisol increase rate (Fig. 14b) for all participants. No obvious correlations between the HR and cortisol with StO2 were observed. Furthermore, no correlation between the

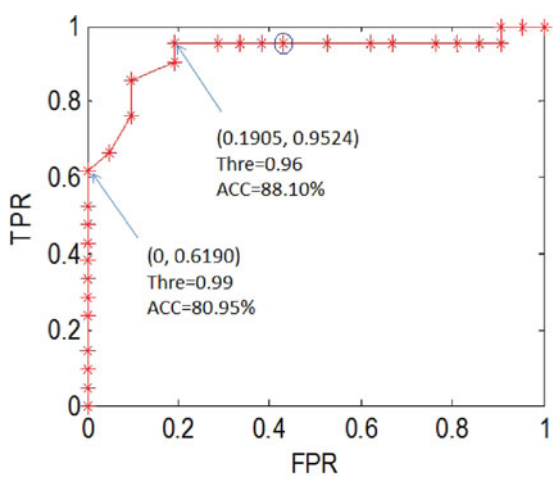

Fig. 13. ROC curve of a binary classifier that used SI as the input.

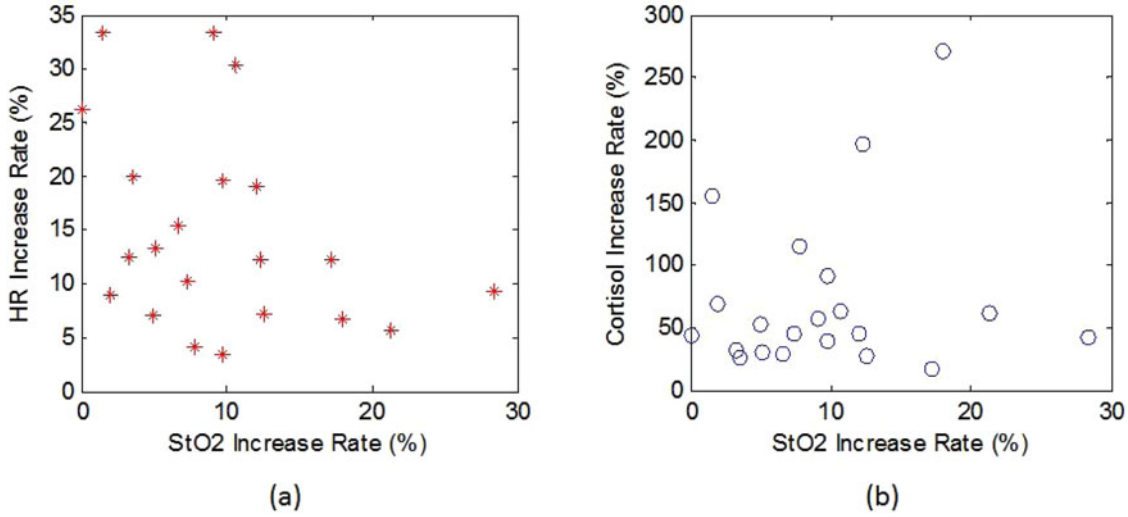

Fig. 14. Scatter plots of (a) StO2 Increase Rate vs. HR Increase Rate; (b)StO2 Increase Rate vs. Cortisol Increase Rate.

forehead StO2 with the HR, which was recorded every 30-60 s during the stress test (Section 7.3), was observed. This result may be a result of the different time scales of the StO2, cortisol, and HR responses.

8 Discussion and Conclusion

We have presented an HSI-based method for the detection of psychological stress. The strong material-discriminating ability of HSI was utilized in this study to differentiate and quantify the amount of blood chromophores (Hb and HbO2) using the Beer-Lambert Law. The manner in which HSI signals are obtained (captured image) characterizes this method as a contact-free stress detection technique.

Facial StO2 is proposed as a feature for stress detection. The elevation of StO2 around specific areas is a physiological response to a stressor. Many researchers have observed this type of elevation, which could be the result of adrenaline secretion in response to stress [42]. Thus, the strategy presented in this paper is a physiological-based stress detection method.

We have demonstrated that HSI StO2 and TI temperature are consistent with each other when measuring blood perfusion. However, HSI StO2 is independent of perspiration and sudden changes in ambient temperature. These characteristics of HSI StO2 make it a robust feature for stress assessment in the case of abrupt ambient temperature alterations. However, transient perspiration can also serve as a stress indicator [32]. In most scenarios, where intense perspiration does not prevail, perspiration is a good stress indicator. In extreme perspiration conditions, HSI StO2 may serve as a complementary feature for stress assessment (e.g., if an individual who experiences heavy sweating must be quickly assessed to determine his/her stress state, and he/she will not recover from intense perspiration until approximately 10 minutes).

We have observed that StO2 is elevated not only around the eye socket area but also around the forehead when individuals respond positively to a psychological stressor. This observation increases the number of ROIs that can be analyzed for stress detection. By normalizing the average forehead StO2, we have developed a SI for detection purposes. The baseline index and SI exhibited a significant difference ($p < 0.005$) and a large practical difference (d=1.37). These results suggest that the HSI StO2 can serve as a new modality to recognize stress at standoff distances.

The HSI StO2 values in this study were obtained from an HSI image cube acquired with still poses. However, by using a more sensitive HSI system (the integration time can be 5 ms) with the ability to image an object at a flexible number of wavelengths, such as an acousto-optic tunable filter based HSI system with scientific CMOS or electron multiplying CCD sensors, an image cube can be obtained in approximately real-time (8 fps if 30 wavelengths are used).The raw HSI data processed to produce an StO2 map included 31 gray images, each of which had the same size as the StO2 map. Thus, the real-time processing substantially depends on a high performance computing system. To facilitate practical application, an effort has been made to reduce the number of gray images required for StO2 map production.

The wavelengths employed to produce StO2 in this study ranged from 518-580 nm. Thus, an illumination source that contains electromagnetic radiation in this specific wavelength range is required.

The detection results presented in this paper are based on stress data from 19 males and two females. The effect of gender on HSI classification results is not currently known, and the results may vary if stress data from more female participants are included.

The method presented in this paper for stress detection could be dependent on a well-defined context. For example, other affective states, such as excitement, may trigger the elevation of forehead StO2. Out of context, the detection may not provide accurate results. Other features must be combined with StO2 to differentiate affective states with similar StO2 responses.

HR was used as an indicator to record HSI data in this research. Without an HR reference, the HSI data would have been continuously recorded, thereby increasing the computing load. A system capable of non-contact HR monitoring combined with the HSI system would be better-suited for stress detection compared with the HSI system alone.

The experiment conducted in this research involved a TSST, and only participants with a 125 percent higher cortisol level and a 6 bpm higher HR were regarded as stressed candidates. Therefore, the stress detected in this research is a strong affective state and may be stronger compared with the stress induced during lie detection. The validity of the method proposed in this research has not been tested in lie detection.

Acknowledgments

The authors would like to thank Cranfield University for providing imaging facilities and valuable supervision. TC and GL would like to thank for the support from the National Natural Science Foundation of China (Grant No. 61301297) and Key Grant Project of Chinese Ministry of Education (No.311032), TC would like to thank for the support from Natural Science Foundation Project of CQ CSTC (No. cstc2012jjA40063) and the Fundamental Research Funds for the Central Universities (No. XDJK2013A006). T. Chen was with the Department of Informatics and System Engineering, Cranfield University, United Kingdom. P. Yuen is the corresponding author.

References

[1] G. P. Chrousos, "Stress and disorders of the stress system," *Nat. Rev. Endocrinology*, vol. 5, pp. 374–381, 2009.

[2] J. M. Koolhaas, A. Bartolomucci, B. Buwalda, S. F. D. Boer, G. Flugge, S. M. Korte, P. Meerlo, R. Murison, B. Olivier, P. Palanza, G. Richer-Levin, A. Sgoifo, T. Steimer, O. Stiedl, G. V. Dijk, M. Wohr, and E. Fuchs, "Stress Revisited: A critical evaluation of the stress concept," *Neurosci. Biobehavioral Rev.*, vol. 35, pp. 1291–1301, 2011.

[3] R. Lazarus, *Stress and Emotion: A New Syhthesis*. New York, NY, USA: Springer, 2006.

[4] I. Pavlidis and J. Levine, "Thermal image analysis for polygraph testing," *IEEE Eng. Med. Biol. Mag.*, vol. 21, no. 6, pp. 56–64, Nov./Dec. 2002.

[5] L. Lefter, L. J. M. Rothkrantz, D. A. V. Leeuwen, and P. Wiggers, "Automatic stress detection in emergency (telephone) calls," *Int. J. Intell. Defence Support Syst.*, vol. 4, no. 2, pp. 148–168, 2011.

[6] J. Zhai and A. B. Barreto, "Realization of stress detection using psychophysiological signals for improvement of human-computer interactions," in *Proc. IEEE SoutheastCon*, 2005, pp. 415–420.

[7] R. W. Picard, E. Vyzas, and J. Healey, "Toward machine emotional intelligence: Analysis of affective physiological state," *IEEE Trans. Pattern Anal. Mach. Intell.*, vol. 23, no. 10, pp. 1175–1191, Oct. 2001.

[8] T. Chen, P. Yuen, K. Hong, A. Tsitiridis, F. Kam, J. Jackman, D. James, M. Richardson, W. Oxford, J. Piper, F. Thomas, and S. Lightman, "Remote sensing of stress using electro-optics imaging technique," in *Proc. SPIE 7486, Optics and Photonics for Counterterrorism and Crime Fighting V, 748606*, Sep. 2009, doi:10.1117/12.830485

[9] K. Hong, P. Yuen, T. Chen, A. Tsitiridis, F. Kam, M. Richardson, D. James, W. Oxford, J. Piper, F. Thomas, and S. Lightman, "Detection and classification of stress using thermal imaging technique," in *Proc. SPIE 7486, Optics and Photonics for Counterterrorism and Crime Fighting V, 74860I*, Sep. 2009, doi:10.1117/12.830496

[10] C. Kirschbaum, J. C. Prussner, A. A. Stone, L. Federenko, J. Gaab, D. Lintz, N. Schommer, and D. H. Hellhammer, "Persistent high cortisol responses to repeated psychological stress in a subpopulation of healthy men," *Psychosom. Med.*, vol. 57, pp. 468–474, 1995.

[11] H. M. Burke, L. C. Fernald, P. J. Gertler, and N. E. Adler, "Depressive symptoms are associated with blunted cortisol stress responses," *Psychosom. Med.*, vol. 67, pp. 211–216, 2005.

[12] C. Kirschbaum, S. Wust, and D. Hellhammer, "Consistent sex differences in cortisol responses to psychological stress," *Psychosom. Med.*, vol. 54, pp. 648–657, 1992.

[13] P. Ekman and W. V. Friesen, *Unmasking the Face: A Guide to Recognizing Emotions from Facial Clues*. Cambridge, MA:ISHK, 2003.

[14] C. Izard, "Innate and universal facial expressions: Evidence from developmental and cross-cultural research," *Psychol. Bull.*, vol. 115, pp. 288–299, 1994.

[15] P. Ekman, *Universals and Cultural Differences in Facial Expressions of Emotion*. Lincoln, NE, USA: Univ. of Nebraska Press, 1971.

[16] D. F. Dinges, R. L. Rider, J. Dorrian, E. L. McGlinchey, N. L. Rogers, Z. Cizman, S. K. Goldenstein, C. Vogler, S. Venkataraman, and D. N. Metaxas, "Optical computer recognition of facial expressions associated with stress induced by performance demands," *Aviation, Space, Environ. Med.*, vol. 76, no. 6, pp. B172–B182, Jun. 2005.

[17] J. Healey and R. Picard, "Detecting stress during real-world driving tasks using physiological sensors," *IEEE Trans. Intell. Transportation Syst.*, vol. 6, no. 2, pp. 156–166, Jun. 2005.

[18] W. Liao, W. Zhang, Z. Zhu, and Q. Ji, "A real-time human stress monitoring system using dynamic Bayesian network," in *Proc. IEEE Comput. Soc. Conf. Comput. Vis. Pattern Recognit.*, 2005, p. 70.

[19] M. Haak, S. Bos, S. Panic, and L. J. M. Rothkrantz, "Detecting stress using eye blinks and brain activity from EEG signals," presented at the Proc. 1st Driver Car Interact. Interface, Prague, Czech Republic, 2008.

[20] D. Metaxas, S. Venkataraman, and C. Vogler, "Image-based stress recognition using a model-based dynamic face tracking system," in *Proc. 4th Int. Conf. Comput. Sci.*, 2004, vol. 3038, pp. 813–821.

[21] J. Kim, "Bimodal emotion recognition using speech and physiological changes," in *Robust Speech Recognition and Understanding*, M. Grimm and K. Kroschel, Eds. Rijeka, Croatia: I-Tech Education and Publishing, 2007, pp. 265-280.

[22] J. Healey and R. Picard, "SmartCar: Detecting driver stress," in *Proc. 15th Int. Conf. Pattern Recognit.*, 2000, pp. 218–221.

[23] K. H. Kim, S. W. Bang, and S. R. Kim, "Emotion recognition system using short-term monitoring of physiological signals," *Med. Biol. Eng. Comput.*, vol. 42, pp. 419–427, 2004.

[24] M. Z. Poh, D. J. McDuff, and R. W. Picard, "Advancements in noncontact, multiparameter physiological measurements using a webcam," *IEEE Trans. Biomed. Eng.*, vol. 50, no. 1, pp. 7–11, Jan. 2011.

[25] I. Pavlidis, J. Dowdall, N. Sun, C. Puri, J. Fei, and M. Garbey, "Interacting with human physiology," *Comput. Vis. Image Understanding*, vol. 108, pp. 150–170, 2007.

[26] M. Z. Poh, D. J. McDuff, and R. W. Picard, "Non-contact, automated cardiac pulse measurement using video imaging and blind source separation," *Opt. Exp.*, vol. 18, pp. 10762–10774, 2010.

[27] M. Garbey, N. Sun, A. Merla, and I. Pavlidis, "Contact-free measurement of cardiac pulse based on the analysis of thermal imagery," *IEEE Trans. Biomed. Eng.*, vol. 54, no. 8, pp. 1418–126, Aug. 2007.

[28] J. Fei and I. Pavlidis, "Thermistor at a distance: Unobtrusive measurement of breathing," *IEEE Trans. Biomed. Eng.*, vol. 57, no. 4, pp. 988–998, Sep. 2009.

[29] I. Pavlidis, J. Levine, and P. Baukol, "Thermal imaging for anxiety detection," in *Proc. IEEE Workshop Comput. Vis. Beyond Vis. Spectrum: Methods Appl.*, 2000, pp. 104–109.

[30] J. A. Levine, I. Pavlidis, and M. Cooper, "The face of fear," *The Lancet*, vol. 357, p. 1757, Jun. 2001.

[31] I. Pavlidis, N. L. Eberhardt, and J. A. Levine, "Seeing through the face of deception," *Nature*, vol. 415, p. 35, Jan. 2002.

[32] D. Shastri, M. Papadakis, P. Tsiamyrtzis, B. Bass, and I. Pavlidis, "Perinasal imaging of physiological stress and its affective potential," *IEEE Trans. Affect. Comput.*, vol. 3, no. 3, pp. 366–378, Jul.–Sep. 2012.

[33] Wikipedia. (2013). Future attribute screening technology [Online]. Available: http://en.wikipedia.org/wiki/Future_Attribute_Screening_Technology

[34] G. A. Shaw and H. K. Burke, "Spectral imaging for remote sensing," *Lincoln Lab. J.*, vol. 4, no. 1, pp. 3–28, 2003.

[35] P. W. Yuen and M. Richardson, "An introduction to hyperspectral imaging and its application for security, surveillance and target acquisition," *Imag. Sci. J.*, vol. 58, no. 5, pp. 241–253, 2010.

[36] P. Yuen and G. Bishop, "Hyperspectral multiple approach fusion for the long-range detection of low observable objects: MUF2," *Proc. SPIE*, vol. 6396, p. 63960C, 2006.

[37] A. Jubran, "Pulse oximetry," *Critical Care*, vol. 3, no. 2, pp. 11–17, 1999.

[38] M. Wolf, K. Siebenthal, M. Keel, V. Dietz, O. Baenziger, and H. U. Bucher, "Tissue oxygen saturation measured by near infrared spectrophotometry correlates with arterial oxygen saturation during induced oxygenation changes in neonates," *Physiol. Meas.*, vol. 21, pp. 481–491, 2000.
[39] P. Rasmussen, E. A. Dawson, L. N. Johannes, J. Lieshout, N. H. Secher, and A. Gjedde, "Capillary-oxygenation-level-dependent near infrared spectrometry in frontal lobe of humans," *J. Cerebral Blood Flow Metabolism*, vol. 27, no. 5, pp. 1082–1093, 2007.
[40] B. L. Seaward, *Managing Stress: Principles and Strategies for Health and Well-Being*, 5th ed. London, U.K.: Jones & Bartlett, 2005.
[41] F. Jones, J. Bright, and A. Clow, *Stress: Myth, Theory, and Research*, London, U.K.: Prentice-Hall, 2001.
[42] S. L. Skinner and R. F. Whelan, "The circulation in forearm skin and muscle during adrenaline infusions," *Australian J. Exp. Biol.*, vol. 40, pp. 163–172, 1962.
[43] T. Chen, "Hyperspectral imaging for the remote sensing of blood oxygenation and emotions," PhD dissertation, Cranfield Defence Sec., Cranfield Univ., Bedfordshire, U.K., 2012, pp. 27–28.
[44] M. S. Creates and J. Grayson, "The effect of adrenaline and noradrenaline on coronary vascular reserve in the dog," *J. Physiol.*, vol. 309, pp. 557–568, 1980.
[45] H. Ishii, T. Niioka, and H. Izumi, "Circulating adrenaline released by sympathoadrenal activation elicits acute vasodilatation in the rat masseter muscle," *Archit. Oral Biol.*, vol. 54, pp. 486–494, 2009.
[46] P. D. Drummond, "The effect of adrenergic blockade on blushing and facial flushing," *Psychophysiol.*, vol. 34, pp. 163–168, 1997.
[47] P. D. Drummond, "The effect of anger and pleasure on facial blood flow," *Australian J. Psychol.*, vol. 46, pp. 95–99, 1994.
[48] P. D. Drummond and J. W. Lance, "Facial flushing and sweating mediated by the sympathetic nervous system," *Brain*, vol. 110, p. 793–803, 1987.
[49] D. Yudovsky, A. Nouvong, K. Schomacker, and L. Pilona, "Assessing diabetic foot ulcer development risk with hyperspectral tissue oximetry," *J. Biomed. Optics*, vol. 16, no. 2, pp. 0260091–0260098, 2011.
[50] L. C. Cancio, A. I. Batchinsky, J. R. Mansfield, S. Panasyuk, K. Hetz, D. Martini, B. S. Jordan, B. Tracey, and J. E. Freeman, "Hyperspectral Imaging: A new approach to the diagnosis of hemorrhagic shock," *J. Trauma Injury, Infect., Critical Care*, vol. 60, no. 5, pp. 1087–1095, 2006.
[51] K. J. Zuzak, M. D. Schaeberle, E. N. Lewis, and I. W. Levin, "Visible reflectance hyperspectral imaging: Characterization of a noninvasive, in vivo system for determining tissue perfusion," *Anal. Chem.*, vol. 74, no. 9, pp. 2021–2028, 2002.
[52] S. A. Shafer, "Using color to separate reflection components," *Color Res. Appl.*, vol. 10, no. 4, pp. 210–218, 1985.
[53] S. Prahl. (1999, Dec.). Optical absorption of hemoglobin. *Oregon Med. Laser Center* [Online]. Available: http://omlc.ogi.edu/spectra/hemoglobin/
[54] S. Jacques. (2001). Optical absorption of melanin. *Oregon Med. Laser Center* [Online]. Available: http://omlc.ogi.edu/spectra/melanin/index.html
[55] M. S. Holzer, S. L. Best, N. Jackson, A. Thapa, G. V. Raj, J. A. Cadeddu, and K. J. Zuzak, "Assessment of renal oxygenation during partial nephrectomy using hyperspectral imaging," *J. Urol.*, vol. 186, pp. 400–404, 2011.
[56] K. M. Cross, L. Leonardi, J. R. Payette, M. Gomez, M. A. Levasseur, B. J. Schattka, M. G. Sowa, and J. S. Fish, "Clinical utilization of near-infrared spectroscopy devices for burn depth assessment," *Wound Repair Regeneration*, vol. 15, no. 3, pp. 332–340, 2007.
[57] T. Chen, P. Yuen, M. Richardson, Z. She, and G. Liu, "Wavelength and model selection for hyperspectral imaging of tissue oxygen saturation," *J. Imaging Sci.*, submitted for publication.
[58] T. Chen, P. Yuen, K. Hong, I. Ibrahim, A. Tsitiridis, U. Soori, J. Jackman, D. James, and M. Richardson, "Assessment of tissue blood perfusion in-vitro using hyperspectral and thermal imaging techniques," in *Proc 5th Int. Conf. Bioinformat. Biomed. Eng.*, 2011, pp. 1–4.
[59] N. Gupta, R. Dahmani, K. Bennett, S. Simizu, D. R. Suhre, and N. B. Singh, "Progress in AOTF hyperspectral imagers," presented at the Proc. SPIE 4054, Autom. Geo-Spatial Image Data Exploitation, Orlando, FL, USA, 2000.
[60] K. J. Zuzak, M. D. Schaeberle, and M. T. Gladwin, "Noninvasive determination of spatially resolved and time-resolved tissue perfusion in humans during nitric oxide inhibition and inhalation by use of a visible-reflectance hyperspectral imaging technique," *Circulation*, vol. 104, pp. 2005–2910, 2001.
[61] K. Zuzak, R. Francis, J. Smith, C. Tracy, J. Cadeddu, and E. Livingston, "Novel hyperspectral imager aids surgeons," in *Proc. SPIE Newsroom*, Dec. 2008, DOI: 10.1117/2.1200812.1394
[62] P. Yuen, T. Chen, K. Hong, A. Tsitiridis, F. Kam, J. Jackman, D. James, M. Richardson, W. Oxford, J. Piper, F. Thomas, and S. Lightman, "Remote detection of stress using hyperspectral imaging technique," in *Proc IET Digest, 3rd Int. Conf. Imag. Crime Detection Prevention*, 2009, pp. 1–6.
[63] C. Kirschbaum, K. Pirke, and D. Hellhammer, "The 'Trier social stress test'–A tool for investigating psychobiological stress responses in a laboratory setting," *Neuropsychobiology*, vol. 28, nos. 1/2, pp. 76–81, 1993.
[64] S. S. Dickerson and M. E. Kemeny, "Acute stressors and cortisol responses: A theoretical integration and synthesis of laboratory research," *Psychol. Bull.*, vol. 130, no. 3, pp. 355–391, 2004.
[65] C. Kirschbaum and D. Hellhammer, "Salivary cortisol in psychoneuroendocrine research: Recent developments and applications," *Psychoneuroendocrinology*, vol. 19, no. 4, pp. 313–333, 1994.
[66] C. Kirschbaum, "Trier social stress test," in *Encyclopedia of Psychopharmacology*. Berlin, Germany: Springer, 2010.
[67] N. Takai, M. Yamaguchi, T. Aragaki, K. Eto, K. Uchihashi, and Y. Nishikawa, "Effect of psychological stress on the salivary cortisol and amylase levels in healthy young adults," *Archit. Oral Biol.*, vol. 49, pp. 963–968, 2004.
[68] N. Otsu, "A threshold selection method from gray-level histograms," *IEEE Trans. Syst., Man Cybern.*, vol. SMC-9, no. 1, pp. 62–66, Jan. 1979.

Tong Chen received the BE degree in communication engineering from The Second Artillery Command Institute, China, in 2002, the MSc degree in digital sound and vision processing from University of Wales, United Kingdom, in 2006, and the PhD degree from Cranfield University, United Kingdom, in 2013. He is currently an associate professor in Southwest University, China. His research interests include image/signal processing, hyperspectral imaging, and affective computing.

Peter Yuen received the BS degree in physics from the University of London, United Kingdom, in 1982, the PhD degree from Imperial College London, United Kingdom, in 1987. He is currently a reader in the School of Informatics and Systems Engineering, Cranfield University, United Kingdom. His research interests include remote sensing, target tracking, and signal processing. He was elected as a fellow of the Institute of Physics and the Institute of Mathematics and Its Applications in 2002.

Mark Richardson is a professor of electronic warfare, director of research and head of the Department of Informatics and Systems Engineering, Cranfield University, United Kingdom. His research work is in the fields of Infrared Signature Simulation & Modeling and EO&IR Countermeasures. He has written numerous classified and unclassified papers on these subjects and holds a Classified Patent on a novel Infrared camouflage material. He has acted as a consultant and defence analyst on numerous occasions, to both the UK Ministry of Defence and commercial industry.

Guangyuan Liu received the BS degree in physics from Southwest Normal University, the MPhil and PhD degrees both from the University of Electronic Science and Technology of China. He is currently a professor of signal processing, and director of the Lab for Signal and Information Processing in Southwest University, China. His research interests include signal processing, affective computing, and pattern recognition. He has published numerous papers on physiological-signal-based emotion recognition and classification.

Zhishun She received the BE degree in radio engineering in 1986, the MSc degree in circuits, signals and systems both from Southeast University China in 1989. In 2000, he received the PhD degree from the University of Adelaide, Australia. Currently, he is a reader in electronic engineering at Glyndwr University, United Kingdom. His research interests include signal and image processing with applications to remote sensing, radar and medical diagnosis. He is a senior member of the IEEE.